



HAL
open science

Optical constants of tin selenide single crystals in the transparency region

A. Elkorashy

► **To cite this version:**

A. Elkorashy. Optical constants of tin selenide single crystals in the transparency region. Journal de Physique III, 1991, 1 (6), pp.1169-1179. 10.1051/jp3:1991178 . jpa-00248632

HAL Id: jpa-00248632

<https://hal.science/jpa-00248632>

Submitted on 4 Feb 2008

HAL is a multi-disciplinary open access archive for the deposit and dissemination of scientific research documents, whether they are published or not. The documents may come from teaching and research institutions in France or abroad, or from public or private research centers.

L'archive ouverte pluridisciplinaire **HAL**, est destinée au dépôt et à la diffusion de documents scientifiques de niveau recherche, publiés ou non, émanant des établissements d'enseignement et de recherche français ou étrangers, des laboratoires publics ou privés.

Classification

Physics Abstracts

78.20D — 78.20F — 77.20

Optical constants of tin selenide single crystals in the transparency region

A. M. Elkorashy

Faculty of Engineering, Cairo University-Fayoum Branch, Fayoum, Egypt

(Received 5 November 1990, revised 29 January 1991, accepted 20 February 1991)

Abstract. — The transmittance, T , and reflectance, R , of single crystals of SnSe were measured at normal incidence. The refractive index, n , was measured by the prism method in the transparency region. Measurements were performed at room temperature using plane-polarised light with the plane of polarisation parallel to either the a- or b-crystallographic axis, both of which lie in the plane of cleavage. The extinction coefficient k was calculated from the absorption coefficient. The real and imaginary parts of the complex dielectric constant (ϵ_r, ϵ_i) as well as the reflectance and its phase change (R, Φ) were calculated from the values of n and k . It was shown that SnSe single crystals exhibit birefringence. Assuming that SnSe binding is partly ionic and partly covalent, the optical constants were satisfactorily fitted to the model of single effective oscillator.

1. Introduction.

Tin selenide SnSe and the isomorphous compounds SnS, GeS, and GeSe have recently received increasing interest. Several investigations of the physical properties of SnSe single crystals have been carried out in the past. Asanabe [1, 2], Albers *et al.* [3], and Maier and Daniel [4] studied the electrical properties of p-type SnSe. The conduction in these crystals is anisotropic, with the smallest hole mobility parallel to the c-crystallographic axis. The magnetic susceptibility was measured by Baidakov *et al.* [5] and SnSe was found to be diamagnetic. The electroreflectance spectra at room temperature was measured by Tyagai *et al.* [6]. Eymard and Otto [7] determined the dielectric functions of thin cleaved plates by the optical and electron-energy-loss spectroscopy. Mityagin *et al.* [8] measured the lattice reflection spectra in the long-wavelength infrared range while Chandrasekhar *et al.* [9] deduced the dielectric constants from Raman scattering and infrared reflectance measurements. Car *et al.* [10] calculated the band structure using the local empirical pseudopotential method, and Lukeš *et al.* [11] studied the absorption edge of SnSe.

In previous works [12, 13] the optical absorption in SnSe single crystals was studied near the fundamental absorption edge. The results were analysed on the basis of two- and three-dimensional models. Absorption near the fundamental edge was found to be due to indirect forbidden transition with two phonons involved in the process. The temperature dependence of the optical energy gap was studied from room temperature to near liquid nitrogen temperature. For a better understanding of the physical properties of this interesting material,

the paper presented here is devoted to the study of optical constants of SnSe single crystals in the transparency region.

2. Crystal structure.

Tin selenide crystallises with an orthorhombic structure with lattice constants [14, 15] $a = 0.419$, $b = 0.446$ and $c = 1.157$ nm.

It has a centrosymmetrical structure with a D_{2h}^{16} space group [16]. It has a pronounced layer character which gives rise to perfect cleavage perpendicular to the c -axis. This poses some difficulties: for example, we did not succeed in measuring transmittance, reflectance or refractive index with the plane of polarisation parallel to the c -crystallographic axis.

Tin selenide shows a displacive phase transition from the orthorhombic to the cubic phase at 540 °C [17].

3. Experimental details.

All samples were grown by the Bridgman technique. As grown, samples exhibit p-type conductivity with a hole concentration at room temperature of about 10^{17} - 10^{18} cm⁻³. Thin samples for transmittance and reflectance measurements were obtained by cleavage along {001} planes. The surfaces of the cleaved samples were mirrorlike. To account for the anisotropy of the material, measurements were carried out with plane polarised light with the plane of polarisation parallel to either the a - or b -crystallographic axes which lie in the plane of cleavage. The crystallographic orientation of the samples was performed making use of the well developed cleavage planes and of the pronounced dichroism of the material. Also orientation was done by Laue back reflection from the cleavage planes. Both optical and X-ray methods showed excellent coincidence. Measurements were performed at room temperature. The energy range of incident photons extended from 0.5 to 2.5 eV for reflectance and from 0.5 eV to the cut-off for transmittance and in the transparency region from 0.5 to 1.2 eV for refractive index measurements.

4. Methods and results.

4.1 TRANSMITTANCE. — The transmittance was measured by the sample-in sample-out method.

The transmittance spectral response was measured at normal incidence for several samples with different thickness. All samples exhibited a transmittance cut-off with the cut-off energy for the a -axis greater than for the b -axis. The transmittance cut-off energy was found to be dependent on the thickness of the sample, it increased as the thickness decreased. Figure 1 shows the transmittance spectral response at room temperature for the two directions of polarisation parallel to the a - and b -crystallographic axes. The thickness of the sample used for this figure is 125 μm.

4.2 REFLECTANCE. — The reflectance was measured by the comparison method, in which the intensity of light reflected by the sample is compared with that reflected by a standard reference of known reflectance. The reference which we used was an optically polished Ge single crystal (n-type with resistivity equal to 52 Ω cm).

The reflectance spectral response was measured at an angle of incidence which did not exceed 15°. All samples exhibited a more or less sharp rise in reflectance towards the lower photon energy. Figure 2 shows the reflectance spectral response at room temperature for the a - and b -axes using the same sample of figure 1 with thickness 125 μm. Each sample is considered as a strip of nearly parallel surfaces, whose thickness is several wavelengths or

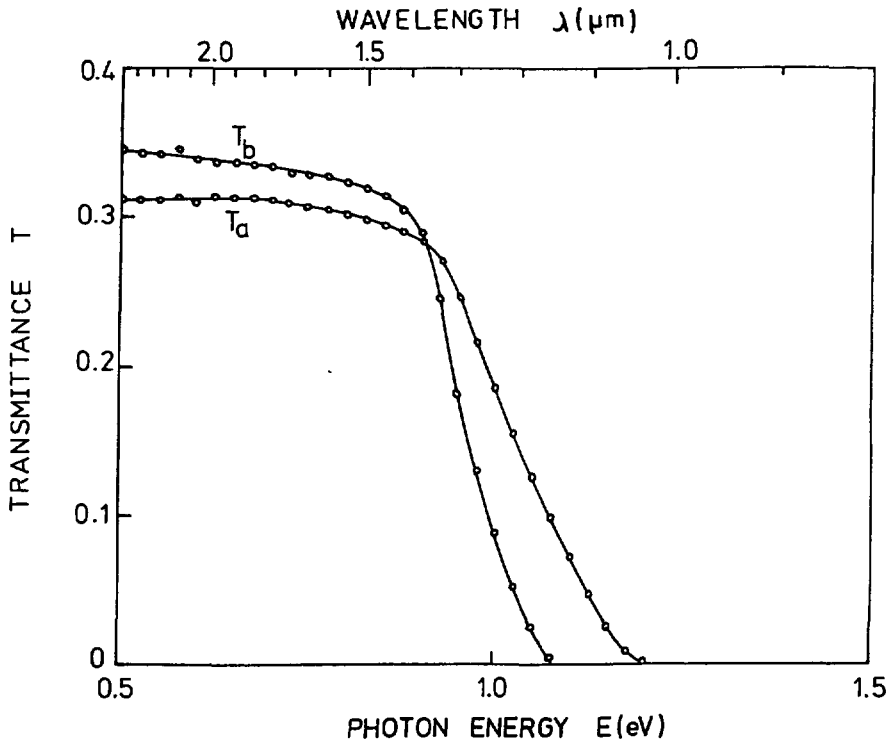


Fig. 1. — The transmittance spectral response for the two directions of polarisation. The thickness of the sample is 125 μm .

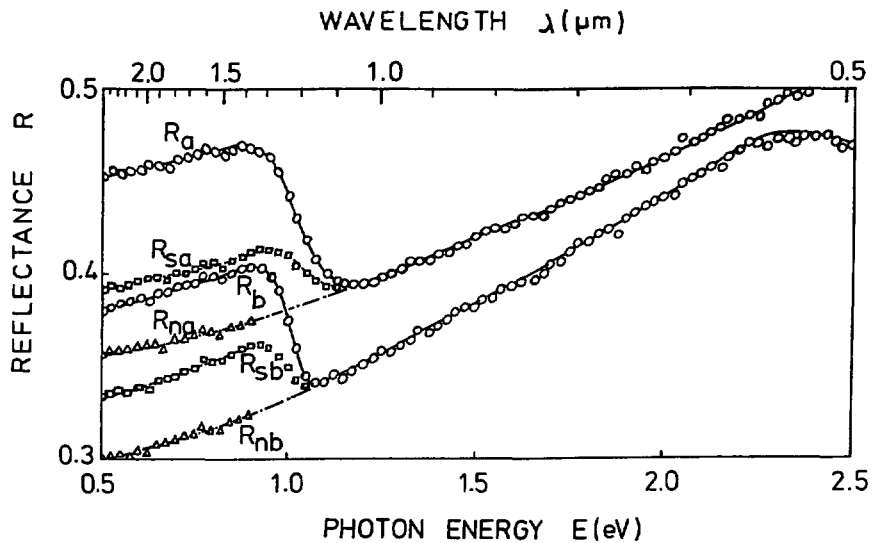


Fig. 2. — The sample (measured), the one-surface and the normalised reflectance spectral responses R , R_s and R_n respectively. (—) measured R ; (---) R_s calculated from equation (3); (—) R_n normalised by multiplying R_s by an E -independent factor. The thickness of the sample is 125 μm .

whose surfaces are not very flat. Under this condition interference effects are not marked, and the intensities of the radiation reflected from the front and back surfaces may be added. The sample reflectance R and the transmittance T at normal incidence of such a sample are given by :

$$R = R_s \left[1 + \frac{(1 - R_s)^2 \exp(-2 \alpha d)}{1 - R_s^2 \exp(-2 \alpha d)} \right] \quad (1)$$

$$T = \frac{(1 - R_s)^2 \exp(-\alpha d)}{1 - R_s^2 \exp(-2 \alpha d)} \quad (2)$$

where R_s is the one surface reflectance or the reflectance of the surface of an infinitely thick slab, α is the absorption coefficient and d is the thickness. Solving equations (1) and (2) simultaneously R_s and α can be calculated from the measured values of R and T . The one surface reflectance can thus be calculated from the measured transmittance and reflectance as

$$R_s = \frac{R}{1 + T \exp(-\alpha d)} \quad (3)$$

Figure 2 shows also the spectral response of R_s . Unfortunately the one surface reflectance R_s did not completely correct the rise in reflectance for back reflection. Values of R_s , calculated from equation (3), were normalised to fit smoothly the measured values of

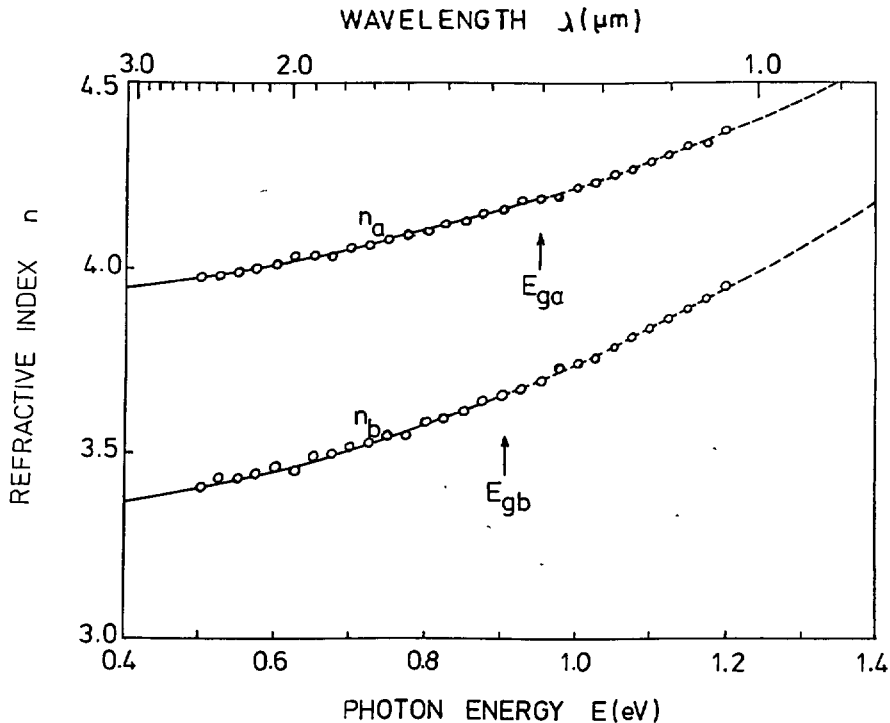


Fig. 3. — The variation of the measured refractive index n , with the photon energy for the a - and b -crystallographic axes. The full curves represent fitting to equation (4a), and the broken curves represent their extensions above energy gap.

R at the high energy side by an E -independent factor. Figure 2 shows also the spectral response of the normalised reflectance R_n .

4.3 REFRACTIVE INDEX. — The refractive index was directly measured by the prism method. For this purpose samples in the form of thin prisms with plane surfaces were used. One face of the prism was natural (cleaved) and the other was ground and optically polished. Three prisms with the two faces intersecting along the b -axis at angles 9, 11 and 12° were prepared. A precision optical goniometer was used with the beam always entering the polished face of the prism and emerging from the natural surface, with the prism aligned so that this surface was strictly perpendicular to the emerging beam. Figure 3 shows the dispersion of the refractive index, n , for the a - and b -crystallographic axes. In the transparency region the refractive index can be expressed by the Cauchy-Sellmaier equation, namely

$$n(E) = n_0 + a_1 E^2 + a_2 E^4 + a_3 E^6 + \dots \quad (4a)$$

or

$$n(\lambda) = n_0 + \frac{a'_1}{\lambda^2} + \frac{a'_2}{\lambda^4} + \frac{a'_3}{\lambda^6} + \dots \quad (4b)$$

The experimental points were fitted to the Cauchy-Sellmaier equation and the least square fitting gave

$$n_a(E) = 3.893 + 0.331 E^2 \quad (4a')$$

$$n_a(\lambda) = 3.893 + 0.509/\lambda^2 \quad (4b')$$

for the a -axis and

$$n_b(E) = 3.299 + 0.449 E^2 \quad (4a'')$$

$$n_b(\lambda) = 3.299 + 0.690/\lambda^2 \quad (4b'')$$

for the b -axis where E is in eV and λ in μm . The coefficients of terms of higher orders were less than 10^{-5} . The full curves in figure 3 represent fittings to equation (4a), and the broken curves represent their extensions above the energy gap. The above results of refractive index show that SnSe exhibits remarkable birefringence.

4.4 OPTICAL CONSTANTS. — The extinction coefficient, k , was directly calculated from the interband absorption coefficient [12]. Figure 4 shows the spectral variation of both n and k in the photon energy range from zero to 1.5 eV for the two directions of polarisation.

Figure 5 shows the spectral variation of the real and imaginary parts ($\epsilon_r = n^2 - k^2$ and $\epsilon_i = 2nk$) of the complex dielectric constant for both a - and b -axes. The reflectance R and the phase change Φ associated with reflection were calculated from the values of n and k by the following equations :

$$R = \frac{(n-1)^2 + k^2}{(n+1)^2 + k^2} \quad (5)$$

and

$$\Phi = \tan^{-1} \frac{-2k}{n^2 + k^2 - 1} \quad (6)$$

Figure 6 shows the spectral variation of the reflectance and the phase change. The solid line is the reflectance calculated from equation (5), the circles are the measured values of reflectance

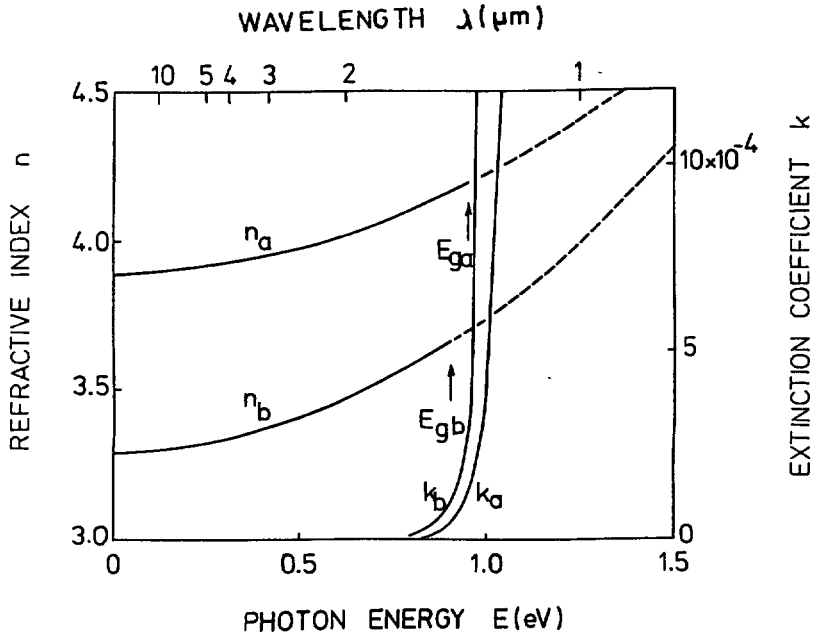


Fig. 4. — The spectral variation of refractive index and extinction coefficient (n and k) for the a - and b -axes.

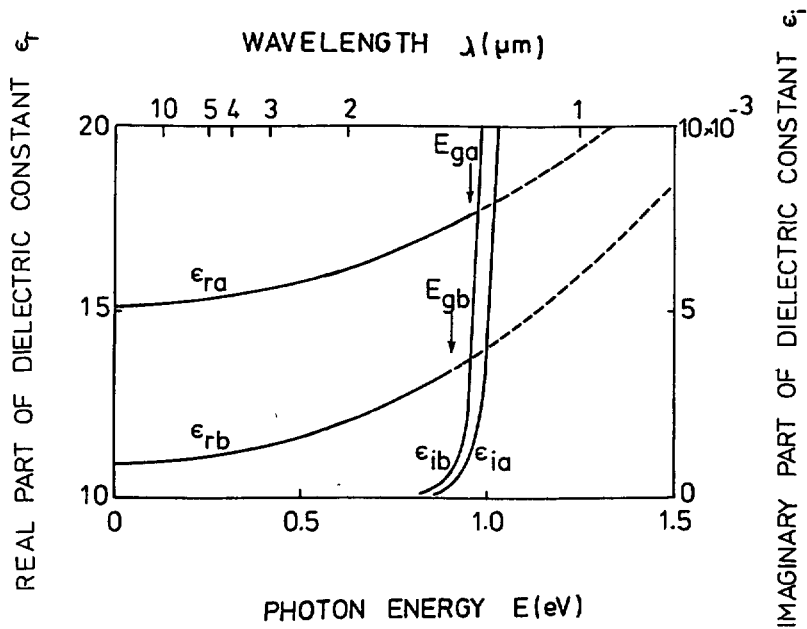


Fig. 5. — The spectral variation of the real and imaginary parts of the complex dielectric constant (ϵ_r and ϵ_i) for the a - and b -axes.

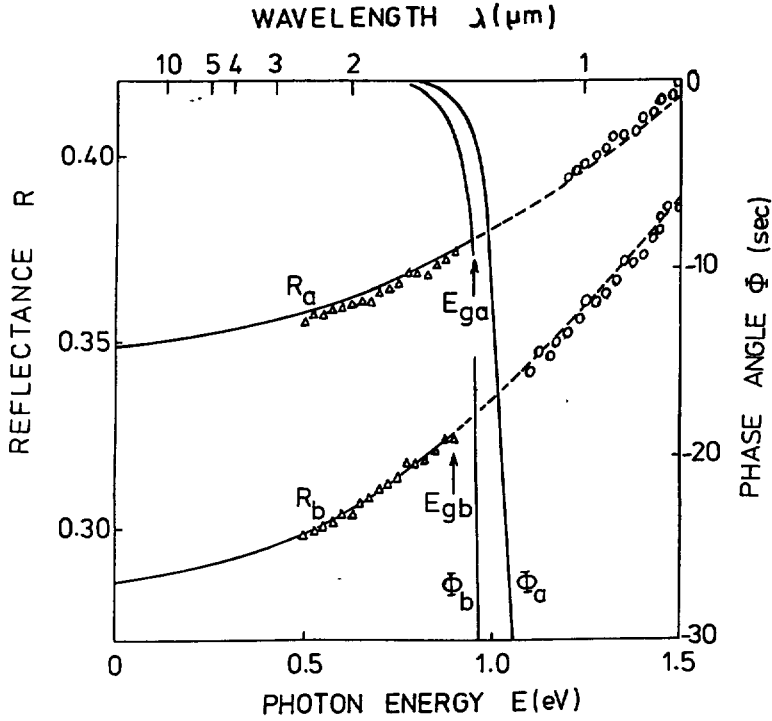


Fig. 6. — The spectral variation of the reflectance and phase change (R and Φ) for the a - and b -axes. The full curves are the reflectance calculated from equation (5), the circles are the measured values of reflectance for $E > E_g$ and the triangles are the normalised reflectance for $E < E_g$.

and the triangles are the normalised reflectance for the two directions of polarisation.

The complex dielectric constant ϵ^* is the optical constant accessible to physical interpretation. Our results of refractive index dispersion below the interband absorption edge correspond to the fundamental electronic excitation spectrum. Wemple and Di Domenico [18] have analysed more than 100 widely different solids and liquids using a single effective oscillator fit of the form :

$$\epsilon_r(E) = 1 + \frac{F}{(E_0^2 - E^2)} \tag{7}$$

where the two parameters E_0 and F are related straightforwardly to the electric dipole strengths and the corresponding transition frequencies of all oscillators. By a special combination of parameters Wemple and Di Domenico defined the parameter E_d as

$$E_d = \frac{F}{E_0} \tag{8}$$

Equation (7), neglecting values of k in the transparency region, now gives

$$\epsilon_r(E) = n^2(E) = 1 + \frac{E_d E_0}{E_0^2 - E^2} \tag{9}$$

They found empirically that

$$E_d = \beta N_c Z_a N_e \quad (10)$$

where N_c is the coordination number of the cation nearest neighbour to the anion, Z_a is the formal chemical valency of the anion, and N_e is the effective number of valence electrons per anion.

We obtained the values of the parameters E_0 and E_d by plotting $(n^2 - 1)^{-1}$ versus E^2 and fitting it to a straight line as shown in figure 7. The solid lines in figure 7 represent the

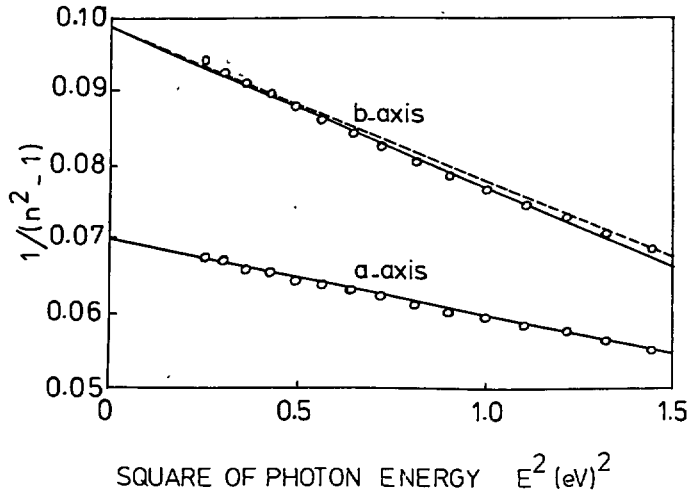


Fig. 7. — $(n^2 - 1)^{-1}$ plotted against E^2 for the a - and b -axes. The circles are the measured values. The solid lines are the least square fit while the dashed line is obtained from equation (4a'') for the b -axis. The solid and dashed lines coincide for the a -axis.

least square fit of the experimental points, and the dashed lines are obtained from equations (4a') and (4a'') for the a - and b -axes respectively. It should be noted that the solid and dashed lines coincide for the a -axis and are slightly deviated for the b -axis. On the basis of the above mentioned model, the single oscillator parameters E_0 and E_d are connected to the imaginary part ϵ_i of the complex dielectric constant, and the -1 and -3 moments of the $\epsilon_i(E)$ optical spectrum, as defined in [18], can be derived from the relations

$$E_0^2 = \frac{M_{-1}}{M_{-3}} \quad (11)$$

$$E_d^2 = \frac{M_{-1}^3}{M_{-3}} \quad (12)$$

Table I gives the values of the single effective oscillator parameters E_0 , E_d , M_{-1} and M_{-3} for the a - and b -crystallographic axes.

In applying equation (10) to SnSe single crystals, there is some uncertainty about the coordination number of the anion which may be thought to be 6 (deformed NaCl structure) or 3 (taking account of the layer structure). The other parameters in equation (10) are well defined, namely $Z_a = 2$, $N_e = 4 + 6 = 10$. The resulting β 's for values of N_c between 3 and 6 are given in table II for the a - and b -axis.

Table I. — *The single effective oscillator parameters.*

	<i>a</i> -axis	<i>b</i> -axis
E_0 (eV)	2.60	2.15
E_d (eV)	37.19	21.82
M_{-1} (dimensionless)	14.29	10.15
M_{-3} (eV ⁻²)	2.11	2.20

Table II. — *Values of the parameter β in equation (10) for various N_c .*

N_c	β (eV)	
	<i>a</i> -axis	<i>b</i> -axis
3	0.62	0.36
4	0.46	0.27
5	0.37	0.22
6	0.31	0.18

5. Discussion of the results.

The reflectance spectral response showed a pronounced rise near the fundamental absorption edge which seems to be common to most of the layer-type materials. Similar rise was observed for GeSe [19-21], GeS [22-25] and for GaS and GaSe [26] single crystals. These crystals belong to the group of layer-type semiconductors.

From equation (4), it can be seen that the refractive index is a monotonically increasing function of E . Since R is related to n by equation (5), we expect R to be also a monotonically increasing function of E . From figure 2, it can be seen that R_s at low energy does not fit the measured values of R at the high energy side of the spectrum. In figure 2, R_s was calculated from equations (1) and (2) which take into consideration the back surface reflection resulting in multiple reflections within the sample. Thus the rise can be explained as partially due to back surface reflection (R_s corrects only 60 % and 55 % of the rise for the *a*- and *b*-axes respectively at $E = 0.9$ eV). By multiplying R_s below $E = 0.9$ eV by an E -independent factor we could have a smooth monotonically increasing reflectance. The remaining part of reflectance (40 % and 45 % for the *a*- and *b*-axes respectively at $E = 0.9$ eV), which is the difference between R_s and R_n , was attributed to internal photon scattering caused by the layer structure of the material. This means that the material under considerations, SnSe, being of pronounced layer-character, causes irregular reflections by the different layers inside the sample which increases the measured reflectance. Equations (1) and (2) take into consideration the back-surface reflection only. Thus we can say that R_s and R_n are the one surface reflectance in presence and in absence of this internal photon scattering caused by the layers respectively. This is clearly seen from figure 6, where the values of the normalised reflectance, R_n and not R_s , coincide with those calculated from the refractive index, equation (5).

Moreover the reflectance spectral response shows a second decrease above the fundamental absorption edge at about 2.2 eV for the b -axis and no similar decrease for the a -axis. This can be interpreted as due to increase in absorption near an energy gap of nearly the same value, which needs to be studied in more detail. This, however, is beyond the scope of the present article. Similar results, namely decrease in reflectance above the fundamental absorption edge for the b -axis and not for the a -axis, were observed with GeSe [19-21] and GeS [22-25].

The refractive index, as shown in figure 3, shows pronounced birefringence with $n_a > n_b$ over the transparency region where the photon energy is smaller than the optical energy gap. The difference between the two refractive indices n_a and n_b converges as the photon energy increases. Similar convergence towards higher energy was observed with GeS [27] while with GeSe [21] the convergence is towards lower energy. The absolute values of the refractive indices obey the relation $n_a > n_b$ in the fundamental electronic excitation range $E < E_g$ with $a < b$. Similar results were obtained with GeSe [21] and with GeS [24, 28] and more general results were found to hold for CdSb [29] and ZnSb [30] namely $n_a > n_b > n_c$ for $E < E_g$ with $a < b < c$. These materials have crystallographic structure similar to that of SnSe.

Wemple and Di Domenico [18] have found empirically that the coefficient β in equation (10) takes the values $\beta_i = 0.26 \pm 0.04$ eV for ionic binding and $\beta_c = 0.37 \pm 0.05$ eV for covalent binding and varies between these two limits for a large number of different materials. By considering these limiting values β_i and β_c , table II shows that the binding in SnSe crystal is partly ionic and partly covalent with the coordination number N_c between 5.0 and 6.0 for the a -axis and between 3.0 and 4.2 for the b -axis. On this basis we come to the conclusion that our results on optical constants fit satisfactorily to the Wemple-Di Domenico model of a single effective oscillator in the considered energy range (from 0.5 to 1.2 eV).

References

- [1] ASANABE S. and OKAZAKI A., *Proc. Phys. Soc. Lond.* **73** (1959) 82.
- [2] ASANABE S., *J. Phys. Soc. Japan* **14** (1959) 281.
- [3] ALBERS W., HAAS C., OBER H., SCHODDER G. R. and WASSCHER J. D., *J. Phys. Chem. Solids* **23** (1962) 215.
- [4] MAIER H. and DANIEL D. R., *J. Electron. Mater.* **6** (1977) 693.
- [5] BAIDAKOV L. A. and KAZAKOVA E. A., *Inorg. Mater.* **13** (1977) 506.
- [6] TYAGAI V. A., BONDARENKO V. N., KRASIKO A. N., BLETSKAN D. I. and SHEKA V. I., *Sov. Phys. Solid State* **18** (1976) 831.
- [7] EYMARD R. and OTTO A., *Phys. Rev. B* **16** (1977) 1616.
- [8] MITYAGIN Yu. A., KUCHERENKO I. V., VODOP'YANOV L. K. and SHTANOV V. I., *Sov. Phys. Solid State* **19** (1977) 1104.
- [9] CHANDRASEKHAR H. R., HUMPHREYS R. G., ZWICK U. and CARDONA M., *Phys. Rev. B* **15** (1977) 2177.
- [10] CAR R., QUARTAPELLE L. and CIUCCI G., *Phys. Stat. Sol. (b)* **86** (1978), 471.
- [11] LUKEŠ F., SCHMIDT E., HUMLIČEK J., DUB P. and KOŠEK F., *Phys. Stat. Sol. (b)* **137** (1986) 569.
- [12] ELKORASHY A. M., *J. Phys. Chem. Solids* **47** (1986) 497.
- [13] ELKORASHY A. M., *J. Phys. Chem. Solids* **50** (1989) 893.
- [14] OKAZAKI A., *J. Phys. Soc. Japan* **11** (1956) 479.
- [15] WYCKOFF R. W. G., *Crystal Structures Vol. 1* (New York : Interscience Publishers) 1963.
- [16] OKAZAKI A., *J. Phys. Soc. Japan* **13** (1958) 1151.
- [17] ZHDANOVA V. V., *Sov. Phys. Solid State* **3** (1961) 1174.
- [18] WEMPLE S. H. and DI DOMENICO M., *Phys. Rev. B* **3** (1971) 1338.
- [19] ELKORASHY A. M., *Physics of Semiconductors 1978*, Inst. Phys. Conf. ser. 43 (1979) p. 817.

- [20] ELKORASHY A. M., *Phys. Stat. Sol. (b)* **135** (1986) 707.
- [21] ELKORASHY A. M., *Phys. Stat. Sol. (b)* **149** (1988) 747.
- [22] ELKORASHY A. M., *J. Phys. C: Solid State Phys.* **21** (1988) 2595.
- [23] ŠTOURAČ L., ZÁVĚTOVÁ M. and ABRAHÁM A., Proc. 12th Int. Conf. Physics of Semiconductors (Stuttgart) 1974, p. 1012.
- [24] GREGORA I., VELICKÝ B. and ZÁVĚTOVÁ M., Proc. 19th Conf. Int. Commission Optics (Prague) 1975, p. 761.
- [25] GREGORA I., VELICKÝ B. and ZÁVĚTOVÁ M., *J. Phys. Chem. Solids* **37** (1976) 785.
- [26] AKHUNDOV G. A., GASANOVA N. A. and NIZAMETDINOVA M. A., *Phys. Stat. Sol. (b)* **15** (1966) 109.
- [27] ELKORASHY A. M., *Physica b* **159** (1989) 171.
- [28] GREGORA I., VELICKÝ B. and ZÁVĚTOVÁ M., *Phys. Stat. Sol. (b)* **104** (1981) 95.
- [29] ZÁVĚTOVÁ M., *Czech. J. Phys. B* **14** (1964) 271.
- [30] ZÁVĚTOVÁ M., *Phys. Stat. Sol.* **5** (1964) K19.